BeBeC-2024-S04

GUIDELINES FOR ACCURATE SOUND SOURCE QUANTIFICATION IN CLOSED-SECTION WIND TUNNELS

Roberto Merino-Martínez[1]

[1]Faculty of Aerospace Engineering, Delft University of Technology.
Kluyverweg 1, 2629 HS Delft, The Netherlands.

Abstract

Experimental aeroacoustic measurements conducted in wind tunnels are crucial for informing the design process of various devices, including aircraft components or wind turbine blades. Whereas closed-section wind tunnels typically offer better aerodynamic conditions compared to their open-jet counterparts, they often introduce challenges related to noisier test environments and the optimal placement of acoustic sensors, such as microphone arrays, within the test section. As advancements in noise reduction measures lead to quieter test models and our knowledge regarding the location of their main noise sources improves, accurately quantifying the sound sources within these models becomes increasingly important. The present manuscript offers valuable guidelines aimed at enhancing the precision of sound source quantification. It provides practical recommendations regarding microphone placement and the utilization of post-processing techniques, such as manipulations of the cross-spectral matrix. The experimental setup consists of an array of 16 microphones in two different configurations (flush-mounted and recessed in cavities). To assess the quantification accuracy, a speaker playing broadband noise at different sound pressure levels outside of the flow serves as a known reference sound source. A wide range of signal-to-noise ratios (SNRs) are achieved by employing different flow velocities and speaker settings. The results indicate that relatively accurate sound source quantification can be achieved with SNRs down to -10 dB. Lastly, a scaling law for the expected quantification error is proposed in terms of the number of microphones within the array and the SNR. In this manner, the experimental setup can be adapted accordingly to obtain the required level of accuracy.

1 INTRODUCTION

Aeroacoustics is a research field of growing relevance as flow-generated noise is a main contributor to the noise emissions of several industrial applications, such as aircraft [1], ground

vehicles [2, 3], and wind turbines [4, 5]. The harmful health effects associated with excessive noise exposure and the ever stricter environmental noise regulations [6] motivate the design of quieter systems. However, in general, the aforementioned systems are considerably complex consisting of multiple noise sources located in different positions and with diverse characteristics. Therefore, in order to reduce noise emissions efficiently, it is crucial to obtain precise information about the location and strength of all noise sources present within these systems.

Phased microphone arrays [7, 8] are commonly employed for this task since, together with acoustic imaging algorithms [9], they enable sound source visualization and provide estimates of the location and strength of the different sound sources present. These devices considerably outperform the use of single microphones for acoustic measurements in environments with high background noise levels, i.e. with a low signal-to-noise ratio (SNR), [10, 11]. This approach is also normally used to evaluate the performance of noise reduction measures [12–15].

To accurately investigate flow-generated noise within the design process, experimental measurements are typically conducted in (aeroacoustic) wind-tunnel facilities [16–18]. The flow conditions in these tests aim to reproduce those present in practice around the test model under analysis in a controlled environment. Despite some practical limitations (mentioned below), aeroacoustic experiments in wind tunnels enable testing complex models with a high level of small-scale details (such as landing gears [15, 19]) and to quickly shift between operational conditions and configurations for parametric studies. These two benefits make wind tunnel testing an interesting complementary approach compared to other alternatives, such as computational aeroacoustics simulations, which can become prohibitively expensive when considering small-scale details or multiple configurations. Generally speaking, wind tunnel facilities can be divided into two main categories [9, 20, 21] depending on their type test section:

- **Open-jet wind tunnels:** are characterized by the formation of a jet shear layer from the wind-tunnel nozzle's exit. The main advantages of this configuration are that the microphones and other instrumentation can be placed non-intrusively outside the flow (avoiding the interaction with turbulence) and that the background noise levels are typically lower than in the closed-section counterparts. Moreover, the test chamber surrounding the jet can be acoustically treated with acoustic-absorbing foam wedges, so that most sound reflections are suppressed [22]. These benefits usually make this type of configuration preferred in case accurate far-field sound pressure levels (L_p) estimates are of interest [18]. On the other hand, due to the jet spreading, the flow quality and alignment are generally more difficult to control, and corrections are required for obtaining the effective angle of attack and effective aerodynamic coefficients [23, 24]. Acoustic effects, such as the refraction through the shear layer [25], also need to be accounted for, especially when considering the distortion in the phase of the acoustic signals recorded by microphones [26, 27] and the spectral broadening due to the shear layer turbulence [28].

- **Closed-section wind tunnels** normally involve lower corrections for model blockage and circulation with relatively better-controlled aerodynamic properties compared to the open-jet case. Acoustic measurements can be performed non-intrusively by mounting microphones flush-mounted in the floor, ceiling, or walls of the wind tunnel [29], see Fig. 1 (left). However, the amplitudes of the near-field pressure fluctuations inside the turbulent boundary layer (TBL) developing along the wind tunnel's floor, ceiling, or walls are generally much higher than the acoustic signals from the model. Additional challenges

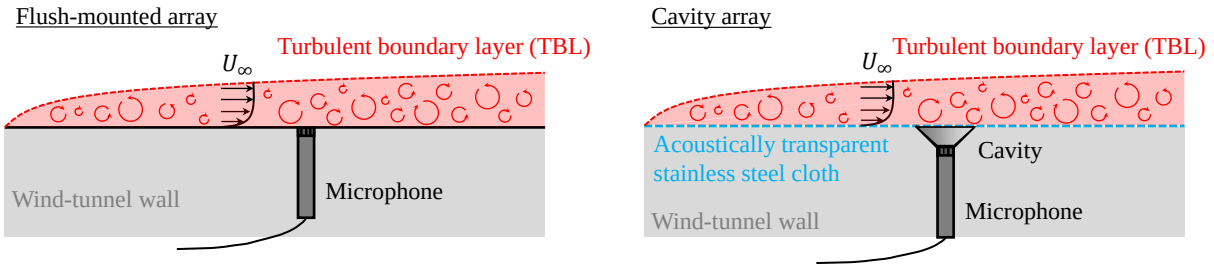

Figure 1: Diagram explaining the two considered configurations for placing microphones on a wind tunnel wall (or floor or ceiling): (left) flush-mounted microphones, (right) recessed microphones in cavities covered by an acoustically transparent cloth [33].

present in this test section configuration involve typically high background noise levels from the wind-tunnel circuit [30] and sound reflections from the solid surfaces of the test section. Overall, these phenomena can lead to erroneous measurements of the absolute sound levels emitted by the model [31, 32].

A compromise solution is a *hybrid* wind tunnel configuration, which involves the replacement of the hard wind-tunnel walls of the closed-section configuration with acoustically transparent walls, such as tensioned Kevlar sheets [14, 34, 35], perforated plates, or wire meshes [33]. By recessing the microphones in cavities covered by such an acoustically transparent wall, the effect of the TBL pressure fluctuations can be substantially attenuated [11, 36–39], see Fig. 1 (right). Therefore, this hybrid test section configuration has the advantages of both closed-section (better controlled aerodynamic properties) and open-jet wind tunnels (placement of the microphones and instrumentation outside the flow). Therefore, a partial conversion of currently existing closed-section facilities into hybrid wind tunnels can be achieved by replacing one (several) of its hard surfaces [40, 41] to enhance the aeroacoustic microphone-array measurement capabilities. This is a considerably simpler and more cost-effective approach than a full refurbishment of the facility.

A recent study by Sanders *et al.* [21] compared airfoil trailing-edge noise measurements conducted in three test section configurations (closed, open-jet, and hybrid) in the same wind tunnel facility and observed L_p differences within ± 3 dB between the far-field noise levels measured with a microphone array[1] in each configuration. The PhD thesis of Kröber [20] investigated the comparability of microphone array measurements in open-jet and closed-section wind tunnels and observed L_p deviations up to 4.6 dB in individual one-third-octave frequency bands.

Given these reported discrepancies, the objective of the current study aims to provide practical guidelines for accurate sound source quantification in close-section wind-tunnel measurements. In particular, recommendations in terms of the minimum number of microphone channels and SNR values required for reliable results in different test conditions are outlined. This manuscript employs the same experimental setup (see section 2) from the study performed by VanDercreek *et al.* [39], which evaluated different cavity geometries to recess the array microphones. For this study two array configurations are evaluated: flush-mounted (baseline) and the

[1]The microphone array distribution was modified for the closed-section configuration.

best-performing cavity geometry proposed by [39]. This investigation also complements previous work [33] on the performance of different advanced acoustic imaging methods for source localization and quantification using the same setup.

The manuscript is structured as follows. Section 2 explains the experimental setup employed. The acoustic imaging method considered is briefly described in section 3. The main results obtained are presented and discussed in section 4 and the conclusions are listed in section 5.

2 EXPERIMENTAL SETUP

2.1 Wind-tunnel facility

The experiments were conducted in the anechoic open-jet wind-tunnel facility of Delft University of Technology (A-tunnel) [22]. The wind tunnel was equipped with a nozzle with a rectangular outlet of 400 mm $\times$ 700 mm, providing a contraction ratio of 15. Even if this facility is an open-jet wind tunnel, this experimental setup aimed to replicate the test conditions present in practice for microphone arrays in closed-section wind tunnels, such as a TBL development along the wall. This was achieved by extending one of the short edges of the rectangular nozzle with an 1100 mm $\times$ 400 mm flat poly-carbonate plate in which the microphones were mounted, see Fig. 2(a). With this configuration, the sound recorded by the microphones is dominated by the TBL noise over the array, as would be the case in a closed-section wind tunnel. This setup also allowed for the speaker employed as a reference sound signal (see section 2.4) to be placed outside of the flow, avoiding the interaction of the jet flow with the speaker and its support structure, which would cause additional flow-generated unwanted noise sources.

The test section of the A-Tunnel is located within an anechoic plenum that measures 6.4 m (length) $\times$ 6.4 m (width) $\times$ 3.2 m (height). The chamber is covered with acoustic absorbing foam wedges, which provide free-field sound propagation properties for frequencies higher than 200 Hz [22]. Flow velocities U_∞ of 20 m/s and 34 m/s were considered for this experiment. Previous hot-wire anemometry measurements in relevant locations on the array support plate confirmed that the boundary layer was indeed turbulent and attached for both flow velocities and both array configurations considered. For more detailed information the reader is referred to [39].

Figure 2(a) also explains the coordinate system used henceforth, centered in the array's center (which is also aligned with the jet axis), with the x axis in the streamwise direction, the y axis pointing right from behind the array, and the z axis pointing towards the jet axis and the speaker.

2.2 Microphone array

The phased array employed consists of 16 *G.R.A.S. 40PH* analog free-field microphones [42] with two additional flush-mounted reference microphones at (x, y) = (-0.4 m, 0 m) and (x, y) = (0 m, 0 m), see Fig. 2(a), which are not used for this study. The microphone array was installed in the aforementioned 1100 mm $\times$ 400 mm poly-carbonate support plate flush-mounted to one of the exit edges of the nozzle, see Fig. 2(a).

The microphone configuration was optimized in a sunflower pattern [43] with a diameter of approximately 350 mm, see Fig. 2(b). The selected microphone configuration is meant to minimize sidelobes, and hence maximize the dynamic range, between 2 kHz and 4 kHz. This design was predicted to have a maximum dynamic range of 9.6 dB and, due to its relatively

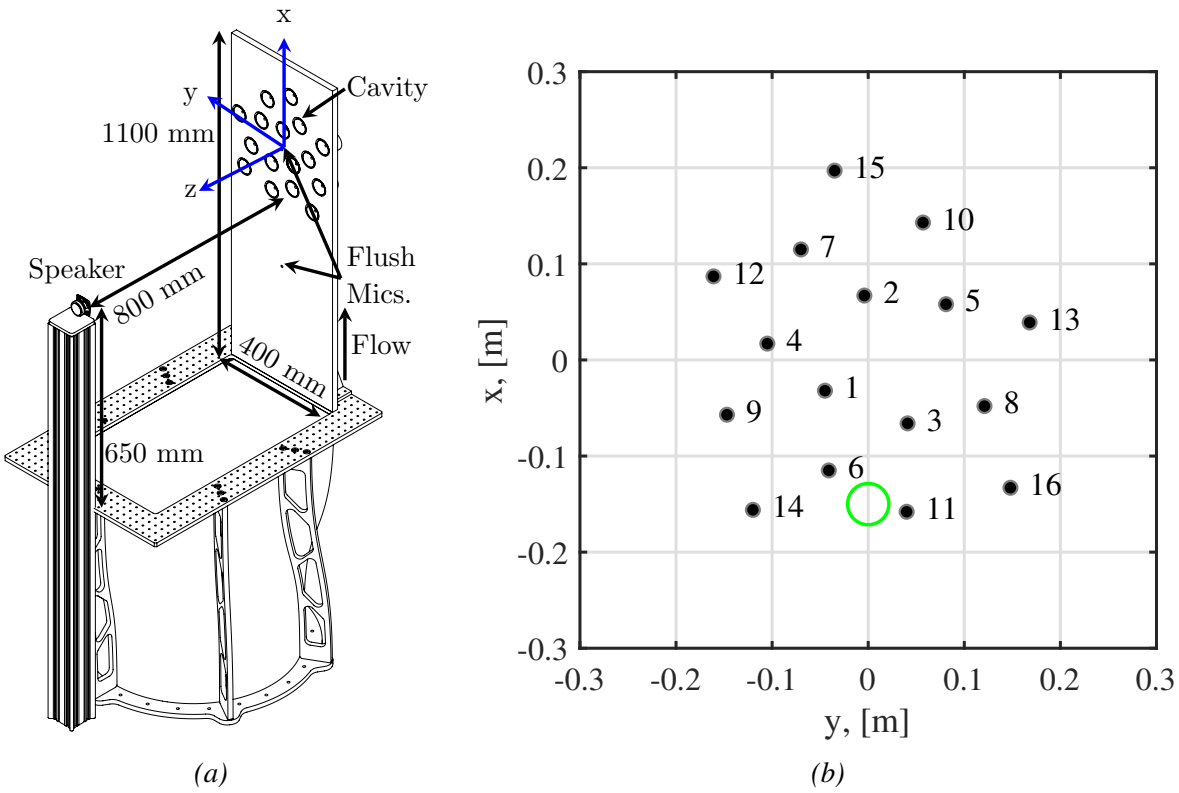

Figure 2: (a) Experimental setup at the A-tunnel with the microphone array installed on the support plate flush-mounted to one of the exit edges of the nozzle. (b) Microphone distribution including the microphone numbering, as seen from the back of the plate. The green circle denotes the relative position of the speaker baffle (placed 800 mm away in the z direction from the array plane). Adapted from [39].

small size, a usable frequency range from approximately 1 kHz to 9.2 kHz [39]. The center of the microphone distribution ($x = y = z = 0$ m) is located 800 mm downstream of the nozzle exit plane, see Fig. 2(a), to enable the boundary layer along the plate to become fully turbulent.

Figure 2(b) also shows the microphone channel numbering employed. Henceforth, to study the influence of the number of microphones N_{mic} employed in the postprocessing analysis, the data recorded by different microphones will be virtually removed sequentially, starting from microphone number 1, then microphones 1 and 2, etc. until microphones 1 to 12 are removed (i.e. only microphones 13-16 remain). Since the latest microphones remaining correspond to those on the outer perimeter of the array, the spatial resolution is expected to stay relatively constant, while the dynamic range is expected to worsen gradually.

All microphones were calibrated individually using a *G.R.A.S. 42AA* pistonphone [44] following the guidelines provided by Mueller [16]. The microphones have a flat frequency response within ± 1 dB from 50 Hz to 5 kHz and within ± 2 dB from 5 kHz to 20 kHz. The data acquisition system consisted of four *National Instruments* (*NI*) *PXIe-4499* sound and vibration modules with 24-bit resolution. The boards are controlled by a *NI RMC-8354* computer via a *NI PXIe-8370* board. The sampling frequency was 51.2 kHz and the recording time was 45 s.

For each frequency analyzed, the cross-spectral matrix (CSM) is calculated using 4096 samples with a 50% overlap using Hanning windowing. The scan grids employed were located at the speaker baffle plane ($z = 800$ mm) and had dimensions of 1 m $\times$ 1 m centered at the expected source location (i.e. for x between -0.6 m and 0.4 m for y between -0.5 m and 0.5 m, see section 2.4. The spacing between neighboring grid points was $\Delta x = \Delta y = 1$ mm. The acoustic spectra, shown in subsequent sections in one-third-octave bands, are presented for the frequencies between 1 kHz and 10 kHz, due to the array and speaker limitations.

2.3 Microphone cavities

Two different array configurations [39] were employed, each of them mounted in a different plate of the same dimensions (1100 mm $\times$ 400 mm):

1. A reference configuration with the microphones flush-mounted to the poly-carbonate plate with holes of the same diameter as the *G.R.A.S. 40PH* microphones (7 mm).

2. A configuration with recessed cavities covered with an acoustically transparent stainless steel cloth with a thread diameter of 0.025 mm and 500 thread per square inch (#500). In this plate, the cavities are installed in threaded holes of 50 mm diameter at the microphone positions, see Fig. 2(a). This configuration allowed for different cavity geometries to be tested [39]. The cavities considered in this paper are derived from a confidential design and have a conical shape with their walls made of sound-absorbing melamine foam.

2.4 Sound source

A single Visaton K 50 SQ speaker [45] was employed as a reference known sound signal. It was placed 800 mm away from the array plane in the z direction and 650 mm downstream from the nozzle outlet (i.e. at $x = -150$ mm) and aligned with the jet axis (i.e. $y = 0$ mm), see Fig. 2a. This corresponds to an observing angle from the array center ($x = y = 0$) of approximately 10.8°. This position is outside the flow to avoid unwanted additional noise sources due to shear layer impingement. The speaker has a baffle diameter of 45 mm, an effective piston area of 12.5 cm^2, and a maximum power of 3 W. Its recommended frequency response range is between 250 Hz and 10 kHz.

The speaker was employed to emit a broadband noise signal at three different overall sound pressure levels ($L_{\text{p,overall}}$) to obtain different SNR scenarios. The average $L_{\text{p,overall}}$ values for the frequency range of interest (1 kHz to 10 kHz) measured by all 16 microphones (without flow) for both arrays configurations and three speaker settings (Low, Mid, and High) are gathered in Table 1. The $L_{\text{p,overall}}$ for the Mid and High speaker settings are approximately 20 dB and 28 dB higher, respectively, than for the Low case. The discrepancies between the values measured by each array configuration (about 6.6 dB) are assumed to be due to the different sound reflection characteristics in each setup: hard wall in the flush-mounted array and a cone made of sound-absorbing melamine foam for the cavity array [39]. Henceforth, the respective frequency spectrum measured in each case (array configuration and speaker setting) is used as a ground truth reference with respect to the test cases with flow.

The measured one-third-octave band spectra averaged for all 16 microphones of each speaker $L_{\text{p,overall}}$ setting (without flow), are depicted in Figs. 3(a) and 3(b) for the flush-mounted and

Table 1: Overall average sound pressure level $L_{p,overall}$ for the frequency range of interest (1 kHz to 10 kHz) values measured by each microphone array configuration for the speaker settings.

	Low	Mid	High
Flush-mounted array	67.1 dB	86.8 dB	94.9 dB
Cavity array	60.5 dB	80.2 dB	88.1 dB

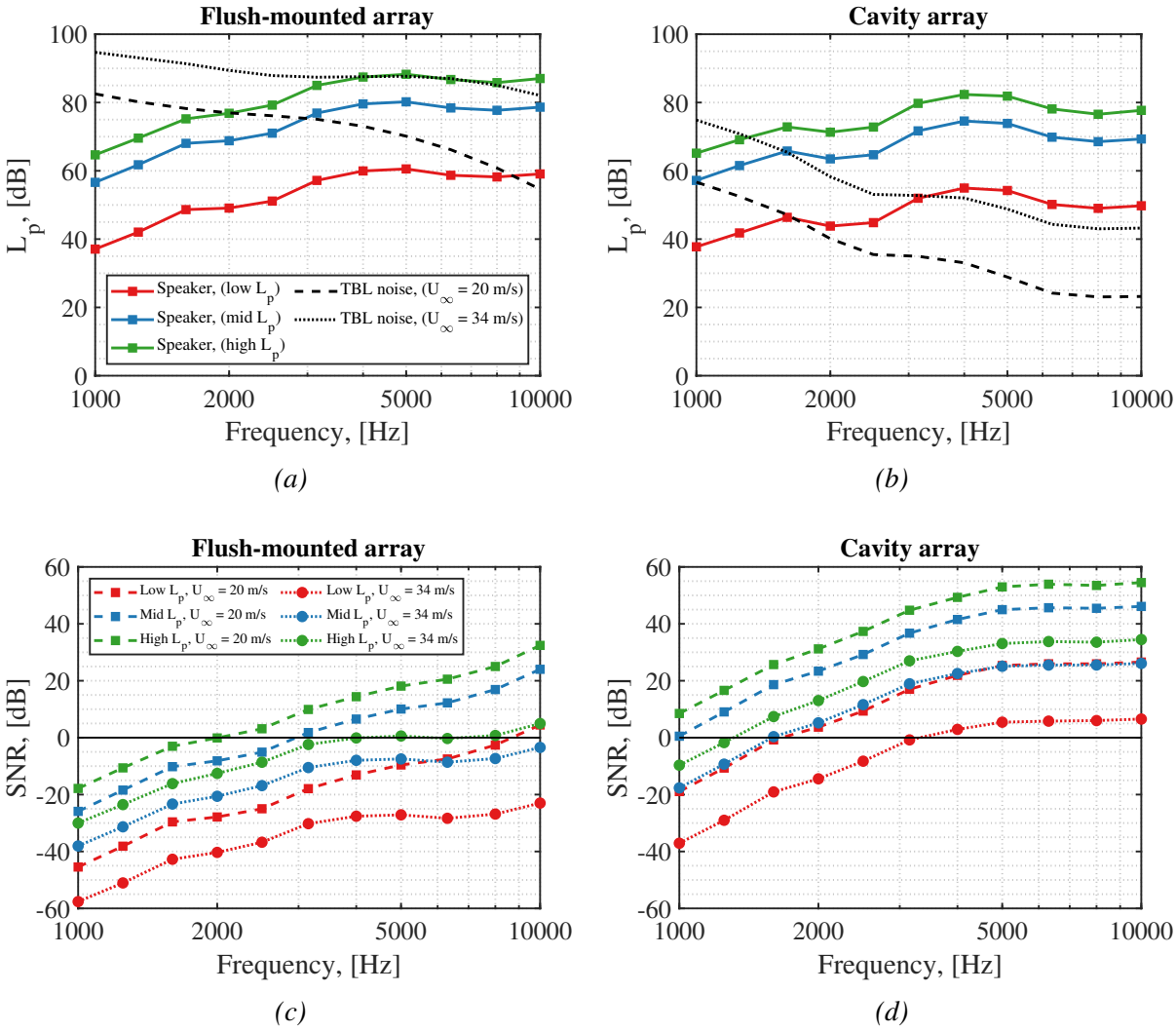

Figure 3: Average one-third-octave band frequency spectra of the speaker (without flow) as well as the TBL noise spectra (with speaker off) for both flow velocities and for the (a) flush-mounted array and (b) cavity array. Signal-to-noise ratio (SNR) of the three speaker signals for both flow velocities and the (c) flush-mounted array and (d) cavity array.

cavity array, respectively. As aforementioned, the cavity array measures lower L_p values than its flush-mounted counterpart, with differences up to about -9.3 dB for the 10 kHz band. In the same subfigures, the TBL average noise spectra for both flow velocities (with the speaker off), is presented as measured by both array configurations. The cavity array effectively reduces the measured TBL noise up to 42 dB for the higher frequency bands compared to the flush-mounted baseline. The reductions of the overall sound pressure level ($L_{p,overall}$) of the TBL noise for the whole frequency range considered (1 kHz to 10 kHz) are 28.5 dB and 23.3 dB for $U_\infty = 20$ m/s and 34 m/s, respectively.

The respective SNR values (defined as $L_{p,speaker} - L_{p,TBL}$) in each case are presented in Figs. 3(c) and 3(d). Overall, the SNR varied considerably for different frequencies, flow velocities, and microphone array configurations, ranging from a minimum of about -57.6 dB, for the flush-mounted array at 1 kHz, speaker setting Low, and 34 m/s, to about 54 dB for the cavity array at 10 kHz, speaker setting High, and 20 m/s. Overall, the cavity array provides SNR increases between 20 dB and 35 dB with respect to the flush-mounted baseline for different frequency bands, see Figs. 3(c) and 3(d).

3 ACOUSTIC IMAGING METHOD

For the current study, conventional frequency domain beamforming (CFDBF) [46] was employed. CFDBF is a method based on the phase differences between the signals recorded by each microphone of the array. This method considers a discretized scan grid of potential sound sources and performs an exhaustive search. That is, for each grid point, the agreement between the expected solution for a potential sound source at that location and the actual signals recorded by the array microphones is assessed. In essence, this process is a directional scanning and the outcome is maximum when a focal position coincides with the location of the actual sound source and smaller elsewhere [46]. This method is widely used since it is robust, intuitive, and relatively computationally inexpensive. However, CFDBF is influenced by the array's point spread function (PSF), i.e. the array's response to a unitary point source, which is limited by the Rayleigh resolution limit, i.e. the minimum distance at which two sound sources can be distinguished, and is subject to high sidelobe levels (spurious sources), especially at high frequencies. To quantify the emissions of a sound source, integration methods, such as the Source Power Integration (SPI) technique and its variants [47], can be employed over the region of integration (ROI) under analysis to reduce the influence of the array's PSF.

For the subsequent analysis, the frequency spectra of the sound emitted by the speaker were calculated by integrating the acoustic source maps within a 200 mm $\times$ 200 mm ROI centered at the speaker, i.e. (x, y) = (-150 mm, 0 mm), see Figs. 5 and 6 as an example.

Some of the shortcomings due to the CFDBF limitations and the challenging test conditions present in closed-section wind tunnels can be (partially) mitigated using postprocessing techniques [9, 48–51]. The use of advanced acoustic imaging techniques is out of the scope of this manuscript, but the interested reader is referred to [33] for a more extended analysis. Overall, since most advanced acoustic imaging methods are based on the CFDBF source maps, it is expected that an improvement in these will also lead to enhanced advanced results.

To minimize the effect of the TBL noise in the recordings made by the microphone array, the main diagonal of the CSM can be removed to eliminate the part of the noise incoherent between microphones. Caution has to be taken to prevent non-physical solutions [9]. An alternative

approach to diagonal removal (DR) is to simply subtract the CSM of the background noise of the wind tunnel (without the speaker on, or the test model installed, in general) from the CSM of the measurement case of interest. The effect of such CSM subtraction is presented in the acoustic source maps Fig. 4(b), where it can be compared to the standard case without DR (Fig. 4(a)), the case with DR (Fig. 4(c)), and the case without flow (Fig. 4(d)) considered as ground truth here. Overall, DR seemed to be the most effective approach in this study and is employed in all the results henceforth.

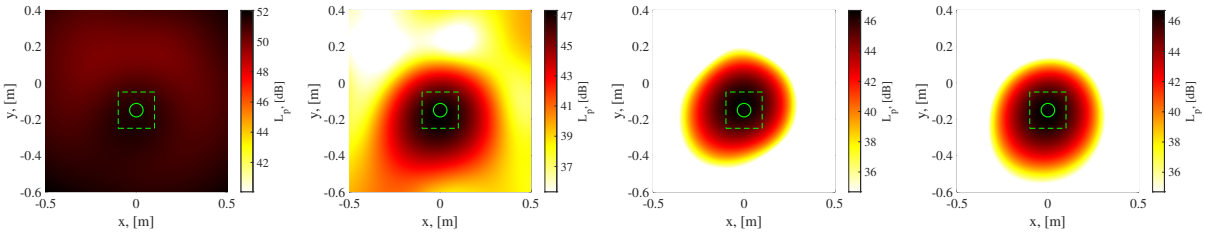

(a) No DR *(b) CSM subtraction* *(c) DR* *(d) No flow*

Figure 4: CFDBF acoustic source maps obtained for cavity array for the speaker emitting the Low L_p value and a one-third-octave frequency band centered at 2000 Hz ($He \approx 2.04$, $SNR \approx -14.5$ dB). (a-c) $U_\infty = 34$ m/s, (d) $U_\infty = 0$ m/s. The dashed green squares denote the ROI and the green circle denotes the speaker baffle.

4 RESULTS AND DISCUSSION

4.1 Acoustic source maps

To illustrate the influence of the number of microphones N_{mic} employed in the post-processing analysis, two sets of exemplary CFDBF acoustic source maps are included in Fig. 5 and Fig. 6 for both array configurations. For both cases, the N_{mic} value considered is sequentially decreased starting from the total of 16 in steps of four, i.e. 12, 8, and 4 microphones. All acoustic source maps have a colour range of 12 dB.

The first example (Fig. 5) corresponds to the speaker emitting the Mid L_{p} value, a flow velocity of 34 m/s and a one-third-octave frequency band centered at 1600 Hz. These conditions provide a SNR value of approximately -23.3 dB and 0.4 dB for the flush-mounted array and the cavity array, respectively. For the flush-mounted array case, (Fig. 5(a-d)) the acoustic source localization capabilities steadily deteriorate with the decreasing N_{mic}, to a point around 8 microphones (Fig. 5(c)) beyond which the speaker can barely be recognized. For the case with four microphones (Fig. 5(d)) the peak L_{p} values in the source map are also around 2 dB higher than for the rest of the cases, indicating some TBL noise contamination. Interestingly, for the cavity array (Fig. 5(e-h)) the localization performance remains somewhat constant with the decreasing N_{mic}. In fact, it seems that the beamwidth (associated with the array spatial resolution) gets narrower as the N_{mic} decreases. Looking at the order in which microphones are virtually removed from the analysis (Fig. 2(b)), the last microphones standing are the ones on the outer perimeter of the array, traditionally attributed for defining the array spatial resolution [52]. On the other hand, for the case with only four microphones (Fig. 5(h)) the dynamic range worsens and sidelobes start appearing on the outer edges of the scan grid considered.

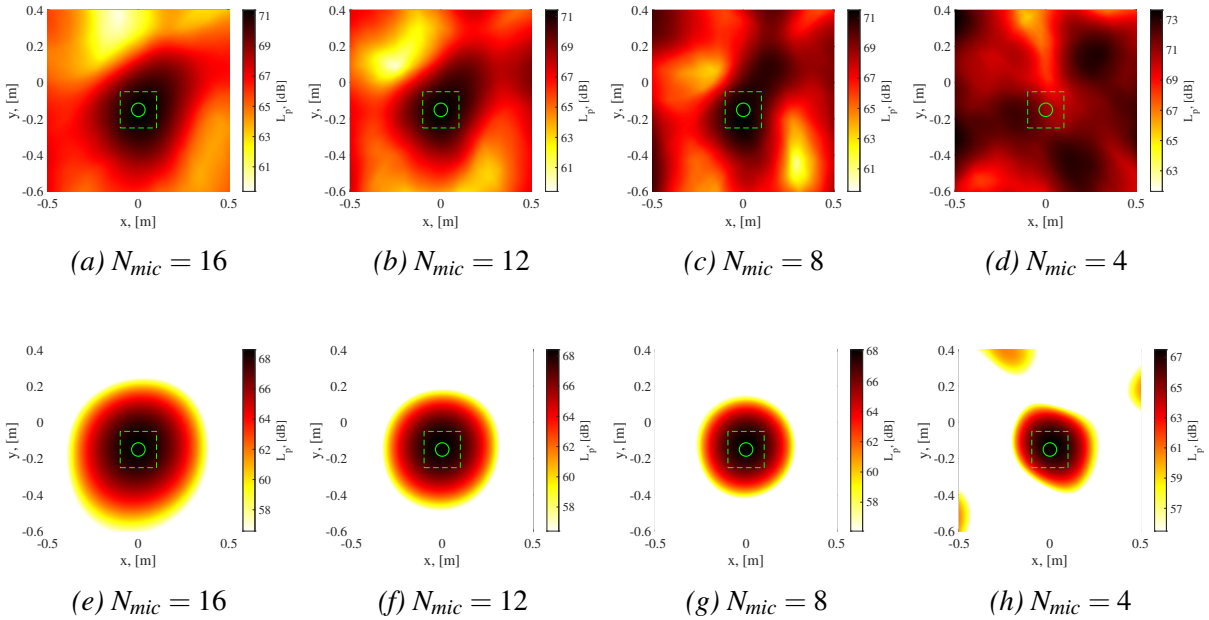

(a) $N_{mic} = 16$ *(b)* $N_{mic} = 12$ *(c)* $N_{mic} = 8$ *(d)* $N_{mic} = 4$

(e) $N_{mic} = 16$ *(f)* $N_{mic} = 12$ *(g)* $N_{mic} = 8$ *(h)* $N_{mic} = 4$

Figure 5: CFDBF acoustic source maps (with DR) obtained for the speaker emitting the Mid L_p value, with $U_\infty = 34$ m/s and a one-third-octave frequency band centered at 1600 Hz ($He \approx 1.63$). (a-d): flush-mounted array (SNR ≈ -27.1 dB), (e-h): cavity array (SNR ≈ 5.4 dB). The dashed blue squares denote the ROI and the green circle denotes the speaker baffle.

Similar trends are observed when assessing the second example (Fig. 6) corresponding to the speaker emitting the Low L_p value, a flow velocity of 34 m/s and a one-third-octave frequency band centered at 5000 Hz. These conditions provide SNR values of approximately -27.1 dB and 5.4 dB for the flush-mounted array and the cavity array, respectively. The even lower SNR value for the flush-mounted array (Fig. 6(a-d)) further hinders the sound source localization, which even offers poor performance when the whole array is considered (Fig. 6(a)). Due to the higher frequency considered in this case, the source maps cavity array (Fig. 6(e-h)) present higher sidelobes early on, and even grating lobes for the case with only four microphones (Fig. 6(h)). The increasing presence of sidelobes can be counteracted by using deconvolution methods, such as CLEAN-SC [53, 54]. Such an approach is out of the scope of this study, a more detailed analysis of the sound source visualization using advanced acoustic imaging methods and the same dataset can be found in [33].

4.2 Influence of the Signal-to-Noise Ratio (SNR)

The SNR between the sound signal to be retrieved and the unwanted background noise level in the wind tunnel (mainly TBL noise in the current case) is expected to be one of the main parameters influencing the accuracy of the sound source quantification.

To evaluate the quantification performance of each configuration considered, the sound pressure level error per one-third-octave band $\Delta L_p = L_{p,measured} - L_{p,exact}$ is employed. This metric represents the difference between the measured L_p values by integrating the acoustic source

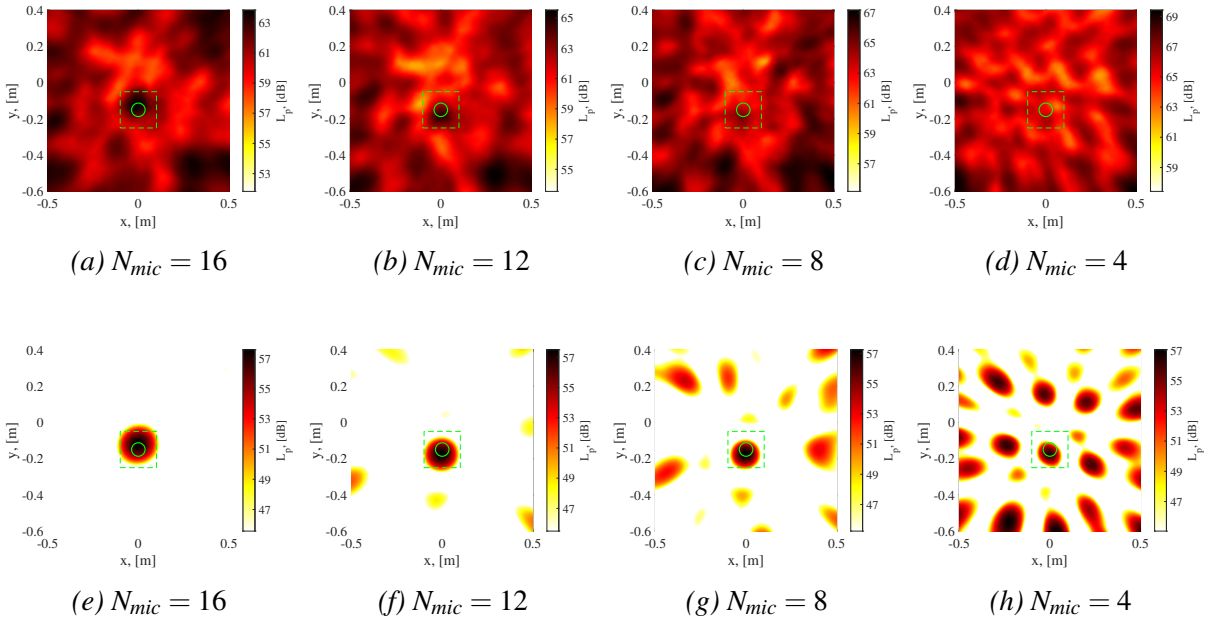

(a) $N_{mic} = 16$ (b) $N_{mic} = 12$ (c) $N_{mic} = 8$ (d) $N_{mic} = 4$

(e) $N_{mic} = 16$ (f) $N_{mic} = 12$ (g) $N_{mic} = 8$ (h) $N_{mic} = 4$

Figure 6: CFDBF acoustic source maps (with DR) obtained for the speaker emitting the Low L_p value, with $U_\infty = 34$ m/s and a one-third-octave frequency band centered at 5000 Hz ($He \approx 5.1$). (a-d): flush-mounted array (SNR ≈ -27.1 dB), (e-h): cavity array (SNR ≈ 5.4 dB). The dashed green squares denote the ROI and the green circle denotes the speaker baffle.

maps (see section 3) and the reference ones measured for each array configuration without flow ($U_\infty = 0$ m/s) considered as *exact*. With this criterion $\Delta L_\mathrm{p} > 0$ corresponds to an overestimation, and vice versa.

Figure 7 depicts the influence of the SNR in the quantification error ΔL_p for different one-third-octave frequency bands when considering the full microphone array (i.e. 16 microphones). For comparison purposes, the non-dimensional Helmholtz number $He = f\,D/c$ is also reported for each case, where f is the sound frequency, D is the array diameter (approximately 350 mm), and c is the speed of sound (here taken as 343 m/s) [8]. The relatively large range of SNR values (roughly from -60 dB to 60 dB) obtained in this experimental campaign thanks to the two array configurations, two flow velocities, and three different speaker settings, provides a total of twelve ΔL_p per frequency band considered.

It can be observed in Fig. 7 that for SNR values higher than -10 dB, the results for different frequencies collapse relatively well showing ΔL_p values within ± 1 dB, which is deemed as acceptable. This seems to indicate that the quantification error is not very dependent on the sound frequency, provided that the SNR is high enough, at least for $1 < He < 10$. For SNR values below -30 dB, the quantification errors quickly increase for decreasing SNR values, up to more than 25 dB discrepancies for the 1 kHz case.

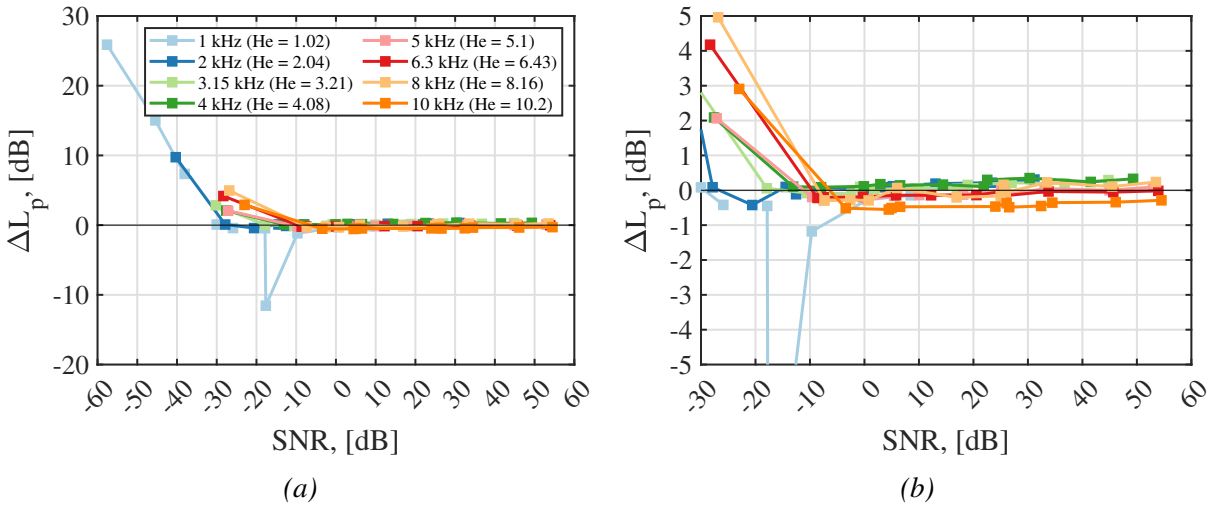

Figure 7: (a) Influence of the SNR in the quantification error ΔL_p for different sound frequencies when using the full microphone array (i.e. $N_{mic} = 16$). (b) Zoomed-in version for SNR values larger than -30 dB.

4.3 Influence of the number of microphones within the array

Another important experimental design parameter, which is normally easier to modify in practice, is the number of microphones N_{mic} employed within the phased array. As previously shown in section 4.1, N_{mic} also has a strong influence on the overall quality of the acoustic source maps obtained, especially in terms of sound source localization accuracy and presence of sidelobes.

Figure 8 presents the ΔL_{p} throughout the frequency range considered for both array configurations and flow velocities evaluated for the speaker setting Low. The results for different numbers of microphones employed from 16 (i.e. full array) to four in steps of two microphones are depicted. In addition, the root-mean-square (RMS) values ε of the ΔL_{p} throughout the frequency range considered (1 kHz to 10 kHz) are also estimated, henceforth, to provide a single quantification metric per case.

In general, the quantification error ΔL_{p} increases for lower frequencies and increasing flow velocities, which corresponds to lower SNR values, see Figs. 3(c) and (d). Moreover, in most cases, removing microphones from the microphone array also leads to higher quantification errors. One exception to this trend is the lower-frequency (1000 Hz and 1250 Hz) results obtained by the cavity array (see Fig. 8(b) and (d)), which are considerably worse when more microphones are employed. In fact, for the case with $U_\infty = 34$ m/s (see Fig. 8(d)), the cases with 10 microphones or less even fail to provide valid results due to the aforementioned non-physical results that DR can cause in some situations. Using a lower N_{mic} value or CSM subtraction instead of DR prevents this issue.

The RMS values of the quantification errors ε for the different number of microphones are presented in a condensed manner in Fig. 9 for the two array configurations, two flow velocities, and three speaker $:_{\text{p}}$ settings. As expected, the cases with lower SNRs (see Fig. 3) present considerably higher ε values. For this analysis, the cases with only two and three microphones were also evaluated for completeness, despite offering very limited acoustic imaging capabilities. In general, increasing N_{mic} monotonically decreases the RMS of the quantification error,

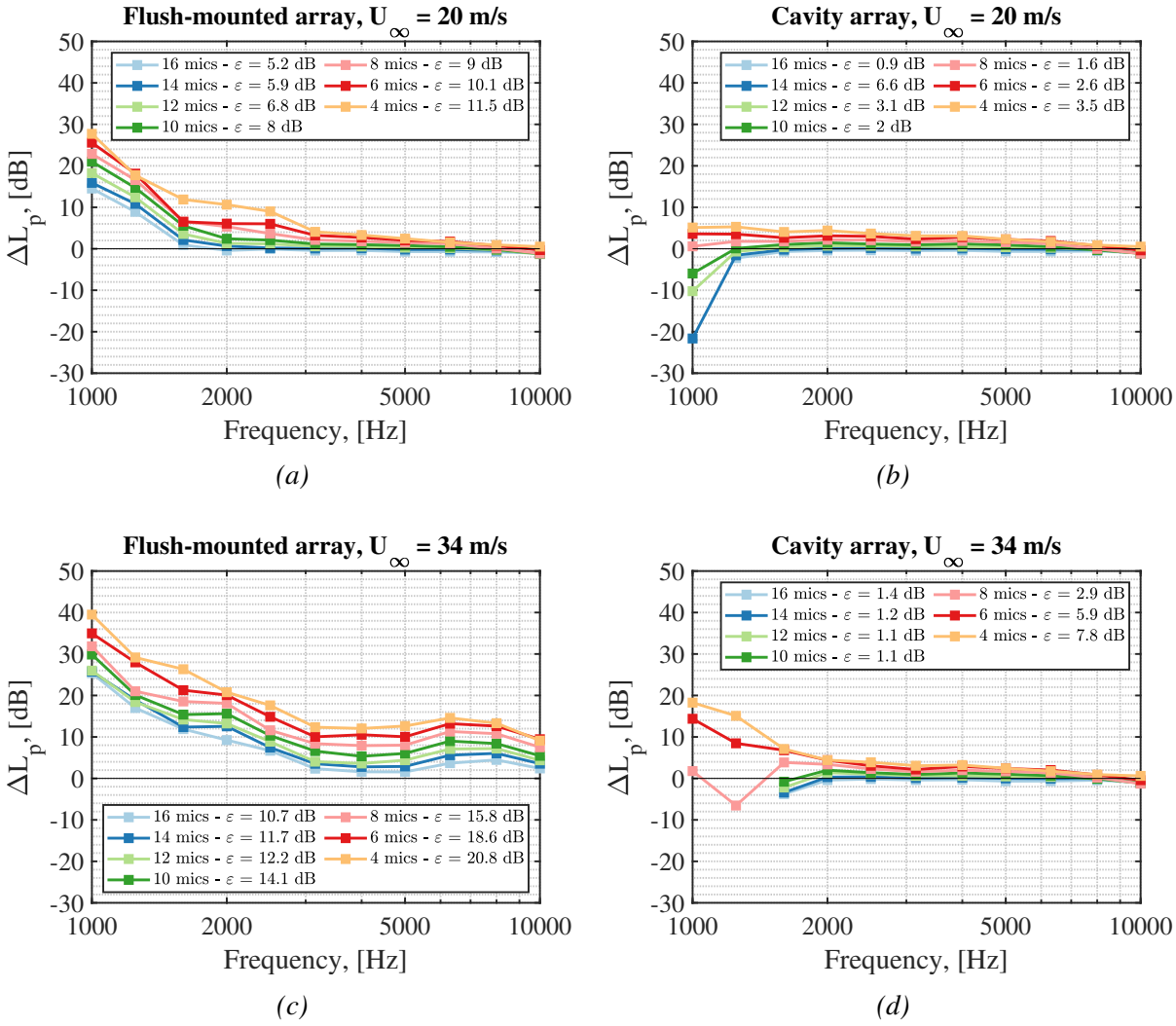

Figure 8: Quantification errors ΔL_p per one-third-octave bands for the speaker emitting the Low L_p setting and for different N_{mic} values. The top row (a,b) corresponds to $U_\infty = 20$ m/s and the bottom row (c,d) to $U_\infty = 34$ m/s. The left column (a,c) corresponds to the flush-mounted array whereas the right one (b,d) refers to the cavity array.

apart from the exceptions mentioned in Fig. 8(b) and (d), in which increasing N_{mic} worsens the results in some situations.

Comparing cases with different SNR values (i.e. different curves in Fig. 9) it seems that for cases with lower SNR values present consistently higher ε values, as expected. In addition, the slope of the curves with respect to N_{mic} seems to increase as well with decreasing SNR, i.e. for cases with low SNR, having additional microphones becomes more crucial. On the other hand, for cases with sufficiently high SNR values, such as the cases with the speaker setting High, all the results seem to asymptotically converge to a single curve.

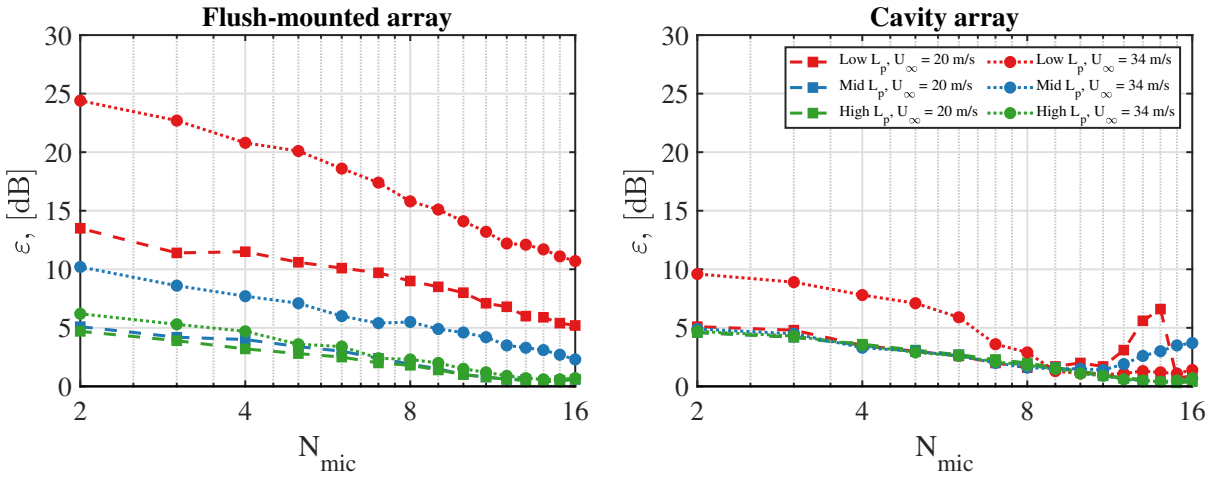

(a) *(b)*

Figure 9: Root-mean-square quantification errors for varying N_{mic} and flow velocities and speaker settings for (a) flush-mounted array and (b) cavity array. Note the logarithmic scale on the horizontal axis.

4.4 Scaling law for quantification error

Based on the available data from this study and the observations made above regarding the influence of SNR and N_{mic}, a general scaling law for the RMS quantification error is proposed, based on those two parameters. It was reported that ε closely follows a logarithmic trend with the inverse of N_{mic}, see Eq. (1):

$$\varepsilon(N_{\text{mic}}, \overline{\text{SNR}}) = k(\overline{\text{SNR}}) \log\left(\frac{1}{N_{\text{mic}}}\right) + C(\overline{\text{SNR}}), \tag{1}$$

where k and C are two variables that depend on the mean SNR of the sound source under study, calculated as the linear average within the frequency range of interest (here denoted as $\overline{\text{SNR}}$). Using least-squares regressions, it was found that the two variables have the following expressions depending on the value of $\overline{\text{SNR}}$ (expressed in dB):

$$k(\overline{\text{SNR}}) = \begin{cases} 0.0011\ \overline{\text{SNR}}^2 - 0.0192\ \overline{\text{SNR}} + 1, & \text{for } \overline{\text{SNR}} < 0 \\ 1, & \text{for } \overline{\text{SNR}} \geq 0, \end{cases} \tag{2}$$

and

$$C(\overline{\text{SNR}}) = \begin{cases} 0.0058\ \overline{\text{SNR}}^2 - 0.0818\ \overline{\text{SNR}} + 3, & \text{for } \overline{\text{SNR}} < 0 \\ 3, & \text{for } \overline{\text{SNR}} \geq 0. \end{cases} \tag{3}$$

The experimental values found for k and C are presented in Fig. 10(a), as well as the proposed expressions in Eqs. (2) and (3), denoted as dashed lines. Following Eqs. (1) to (3), the estimated values of ε for a wide N_{mic} range and three $\overline{\text{SNR}}$ values representative from typical aeroacoustic wind-tunnel experiments are depicted in Fig. 10(b).

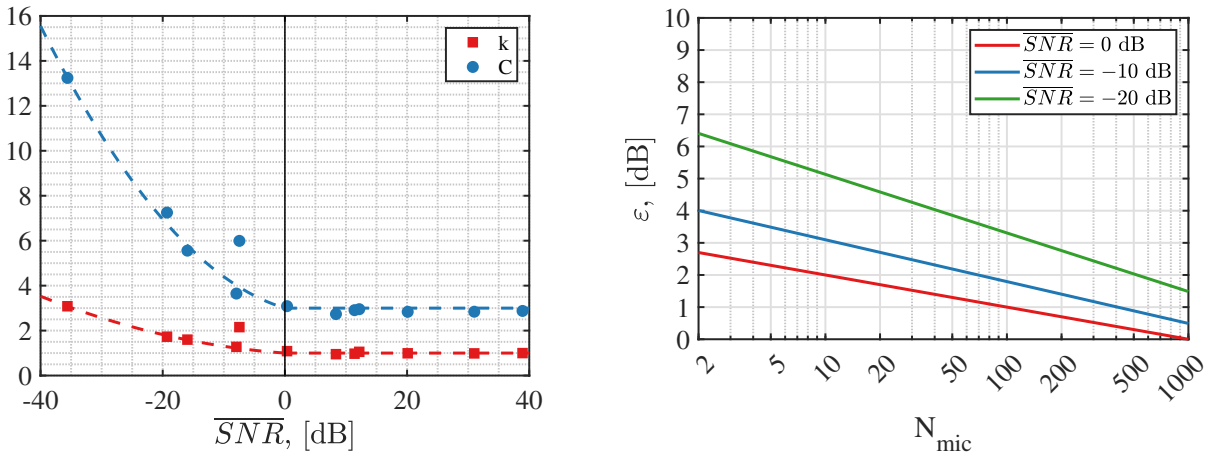

(a) *(b)*

Figure 10: (a) Reported values for the variables k and C for different $\overline{SNR}$ values. The dashed lines represent the proposed expressions in Eqs. (2) and (3). (b) Estimated values of ε for different values of N_{mic} and $\overline{SNR}$, following Eq. (1).

Despite the good agreement of the proposed scaling law for the quantification error with the experimental data in this study, it should be noted that this law has been developed using a limited number of microphones and a relatively small frequency range ($1 < He < 10$). Therefore, this expression is simply provided as a preliminary guideline for the design of aeroacoustic experiments in environments with low SNR.

5 CONCLUSIONS

The current paper investigates the influence that the number of microphones within a phased array and the acoustic environment (represented here as the SNR) have on the accuracy of sound source quantification in aeroacoustic wind-tunnel experiments.

A 16-microphone array in two different configurations and in different flow velocities (i.e. SNR conditions) and was employed with a speaker acting as a known reference sound source to assess the quantification errors in each case. For the frequency range investigated (Helmholtz numbers based on the array diameter between 1 and 10), no clear influence was found between the quantification error and the sound frequency. The SNR and the number of microphones, on the other hand, were reported to strongly influence the accuracy of the results obtained, also in terms of the quality of the acoustic source maps.

Lastly, a scaling law is proposed to estimate the quantification error for different scenarios based on the number of microphones within a phased array and the expected SNR of the sound source of interest. Therefore, the experimental setup can be adapted accordingly to obtain the required level of accuracy.

ACKNOWLEDGEMENTS

The experimental data employed in this work was obtained within the research program THAMES with project number 15215, which is (partly) financed by the Dutch Research Council (NWO). The author kindly acknowledges the contribution of Dr. Colin VanderCreek during the experimental campaign. Additionally, this publication is also a part of the *Listen to the future* project (project number 20247), a part of the Veni 2022 research programme (Domain Applied and Engineering Sciences) granted to Roberto Merino-Martinez and is also (partially) financed by NWO.

References

[1] R. Merino-Martinez, A. Vieira, M. Snellen, and D. G. Simons, *Sound quality metrics applied to aircraft components under operational conditions using a microphone array,* in 25^{th} *AIAA/CEAS Aeroacoustics Conference, May 20 – 24 2019, Delft, The Netherlands* (2019) AIAA paper 2019–2513.

[2] B. Barsikow and M. Klemenz, *Diagnosis of noise sources on high–speed trains using the microphone–array technique,* in *Proc.* 16^{th} *ICA and* 135^{th} *Meeting ASA, Seattle*, Vol. IV (1998) pp. 2229–2230.

[3] P. Bazilinskyy, R. Merino-Martinez, E. Özcan, D. Dodou, and J. C. F. de Winter, *Exterior sounds for electric and automated vehicles: Loud is effective,* **214**, 1.

[4] S. Oerlemans, P. Sijtsma, and B. Méndez López, *Location and Quantification of Noise Sources on a Wind Turbine,* Journal of Sound and Vibration **299**, 869 (2007).

[5] R. Merino-Martinez, R. Pieren, and B. Schäffer, *Holistic approach to wind turbine noise: From blade trailing–edge modifications to annoyance estimation,* Renewable and Sustainable Energy Reviews **148**, 1 (2021).

[6] R. Merino-Martinez, S. J. Heblij, D. H. T. Bergmans, M. Snellen, and D. G. Simons, *Improving Aircraft Noise Predictions by Considering the Fan Rotational Speed,* Journal of Aircraft **56**, 284 (2019).

[7] P. Sijtsma, *Phased array beamforming applied to wind tunnel and fly–over tests*, Tech. Rep. NLR–TP–2010–549 (National Aerospace Laboratory (NLR), Anthony Fokkerweg 2, 1059 CM Amsterdam, P.O. Box 90502, 1006 BM Amsterdam, The Netherlands, 2010).

[8] R. Merino-Martinez, *Microphone arrays for imaging of aerospace noise sources*, Ph.D. thesis, Delft University of Technology (2018), ISBN: 978–94–028–1301–2.

[9] R. Merino-Martinez, P. Sijtsma, M. Snellen, T. Ahlefeldt, J. Antoni, C. J. Bahr, D. Blacodon, D. Ernst, A. Finez, S. Funke, T. F. Geyer, S. Haxter, G. Herold, X. Huang, W. M. Humphreys, Q. Leclère, A. Malgoezar, U. Michel, T. Padois, A. Pereira, C. Picard, E. Sarradj, H. Siller, D. G. Simons, and C. Spehr, *A review of acoustic imaging methods using phased microphone arrays (part of the Aircraft Noise Generation and Assessment special issue), CEAS aeroacoustic journal*, CEAS Aeronautical Journal **10**, 197 (2019).

[10] C. J. Bahr and W. C. Horne, *Subspace–based background noise subtraction applied to aeroacoustic wind tunnel testing,* International Journal of Aeroacoustics **16**, 299 (2017), SAGE Publications Ltd. London, United Kingdom.

[11] C. P. VanDercreek, R. Merino-Martinez, M. Snellen, and D. G. Simons, *Comparison of cavity geometries for a microphone array in a open–jet wind–tunnel experiment,* in 8th *Berlin Beamforming Conference, March 2 – 3 2020, Berlin, Germany* (GFaI, e.V., Berlin, 2020) BeBeC–2020–D7.

[12] C. Arce León, R. Merino-Martinez, D. Ragni, F. Avallone, and M. Snellen, *Boundary layer characterization and acoustic measurements of flow–aligned trailing edge serrations,* Experiments in Fluids **57**, 1 (2016).

[13] A. Rubio Carpio, R. Merino-Martinez, F. Avallone, D. Ragni, M. Snellen, and S. van der Zwaag, *Experimental characterization of the turbulent boundary layer over a porous trailing edge for noise abatement,* Journal of Sound and Vibration **443**, 537 (2019).

[14] R. Merino-Martinez, W. C. P. van der Velden, F. Avallone, and D. Ragni, *Acoustic measurements of a DU96–W–180 airfoil with flow–misaligned serrations at a high Reynolds number in a closed–section wind tunnel,* in 7th *International Meeting on Wind Turbine Noise, May 2 – 5 2017, Rotterdam, the Netherlands* (International Institute of Noise Control Engineering (I-INCE), 1A/B Westminster Chambers, 106 Lord Street, Southport PR8 1LF, United Kingdom, 2017).

[15] R. Merino-Martinez, J. Kennedy, and G. J. Bennett, *Experimental study of realisitic low–noise technologies applied to a full-scale nose landing gear,* Aerospace Science and Technology **113**, 1 (2021).

[16] T. Mueller, *Aeroacoustic Measurements* (Springer Science & Business Media, Berlin, Germany, 2002) p. 313, ISBN: 978–3–642–07514–8.

[17] R. Stoker, Y. Guo, C. Streett, and N. Burnside, *Airframe noise source locations of a 777 aircraft in flight and comparisons with past model–scale tests,* in 9th *AIAA/CEAS Aeroacoustics Conference, May 12 – 14 2003, Hilton Head, South California, USA* (2003) AIAA paper 2003–3232.

[18] J. Pereira Gomes, A. Bergmann, and H. Holthusen, *Aeroacoustic wind tunnel design (part of the Aircraft Noise Generation and Assessment special issue), CEAS aeroacoustic journal*, CEAS Aeronautical Journal **10**, 231 (2019), DOI: 10.1007/s13272-019-00372-7.

[19] R. Merino-Martinez, E. Neri, M. Snellen, J. Kennedy, D. G. Simons, and G. J. Bennett, *Analysis of nose landing gear noise comparing numerical computations, prediction models and flyover and wind–tunnel measurements,* in 24th *AIAA/CEAS Aeroacoustics Conference, June 25 – 29 2018, Atlanta, Georgia, USA* (2018) AIAA paper 2018–3299.

[20] S. Kröber, *Comparability of Microphone Array Measurements in Open and Closed Wind Tunnels*, Ph.D. thesis, Technical University of Berlin (2014).

[21] M. P. J. Sanders, C. F. J. Koenjer, L. Botero-Bolivar, dos Santos F. L., C. H. Venner, and L. D. de Santana, *Trailing–Edge Noise Comparability in Open, Closed, and Hybrid Wind Tunnel Test Sections,* AIAA Journal **60**, 4053 (2022).

[22] R. Merino-Martinez, A. Rubio Carpio, L. T. Lima Pereira, S. van Herk, F. Avallone, M. Kotsonis, and D. Ragni, *Aeroacoustic design and characterization of the 3D–printed, open–jet, anechoic wind tunnel of Delft University of Technology,* Applied Acoustics **170**, 1 (2020).

[23] J. D. J. Anderson, *Fundamentals of Aerodynamics*, Third ed. (McGraw–Hill Series in Aeronautical and Aerospace Engineering, 2001) ISBN: 0–07–237335–0.

[24] J. Barlow, W. Rae, and A. Pope, *Low–Speed Wind Tunnel Testing*, Third ed. (John Willey & Sons, Inc., 1999) ISBN: 0–417–55774–9.

[25] T. Padois, C. Prax, and V. Valeau, *Numerical validation of shear flow corrections for beamforming acoustic source localisation in open wind–tunnels,* Applied Acoustics **74**, 591 (2013).

[26] R. K. Amiet, *Refraction of sound by a shear layer,* Journal of Sound and Vibration **58**, 467 (1978).

[27] D. Ernst, C. Spehr, and T. Berkefeld, *Decorrelation of acoustic wave propagation through the shear layer in open jet wind tunnel,* in 21st *AIAA/CEAS Aeroacoustics Conference, June 22 – 26 2015, Dallas, TX, USA* (2015) AIAA paper 2015–2976.

[28] P. Sijtsma, S. Oerlemans, T. Tibbe, T. Berkefeld, and C. Spehr, *Spectral broadening by shear layers of open jet wind tunnels,* in 20th *AIAA/CEAS Aeroacoustics Conference, June 16 – 20 2014, Atlanta, GA, USA* (2014) AIAA paper 2014–3178.

[29] C. C. J. Pagani, D. S. Souza, and M. A. F. Medeiros, *Slat Noise: Aeroacoustic Beamforming in Closed–Section Wind Tunnel with Numerical Comparison,* AIAA Journal **54**, 2100 (2016).

[30] E. Duell, J. Walter, S. Arnette, and Y. J., *Recent Advances in Large–Scale Aeroacoustic Wind Tunnels,* in 8th *AIAA/CEAS Aeroacoustics Conference, 17 – 19 June 2002, Breckenridge, Co, USA* (2002) AIAA paper 2002–2503.

[31] S. Guidati, C. Brauer, and S. Wagner, *The reflection canceller – Phased array measurements in a reverberating environment,* in 8th *AIAA/CEAS Aeroacoustics Conference and Exhibit, June 17 – 19, 2002, Breckenridge, Colorado, USA* (2002) AIAA paper 2002–2462.

[32] P. Sijtsma and H. Holthusen, *Corrections for Mirror Sources in Phased Array Processing Techniques,* in 9th *AIAA/CEAS Aeroacoustics Conference, May 12 – 14, 2003, Hilton Head, South Carolina, USA* (2003) AIAA paper 2003–3196.

[33] R. Merino-Martinez, C. P. VanDercreek, and M. Snellen, *Evaluation of advanced acoustic imaging methods for microphone–array measurements in closed–section wind tunnels,* in *28th AIAA/CEAS Aeroacoustics Conference, June 14 – 17 2022, Southampton, United Kingdom* (2022) AIAA paper 2022–2810.

[34] B. S. Smith, H. E. Camargo, R. A. Burdisso, and W. J. Devenport, *Development of a Novel Acoustic Wind Tunnel Concept,* in *11th AIAA/CEAS Aeroacoustics Conference, May 23 – 25 2005, Monterey, California, USA* (2005) AIAA paper 2005–3053.

[35] M. C. Remillieux, E. D. Crede, H. E. Camargo, R. A. Burdisso, D. W. J., M. Rasnick, P. van Seeters, and A. Chou, *Calibration and Demonstration of the New Virginia Tech Anechoic Wind Tunnel,* in *14th AIAA/CEAS Aeroacoustics Conference (29th AIAA Aeroacoustics Conference), May 5–7, 2008, Vancouver, British Columbia, Canada* (2008) AIAA paper 2008–2911.

[36] S. M. Jaeger, W. Horne, and C. Allen, *Effect of surface treatment on array microphone self–noise,* in *6th AIAA/CEAS Aeroacoustics Conference, June 12–14 2016, Lahaina, HI, USA* (2000) AIAA paper 2000-1937.

[37] V. Fleury, L. Coste, R. Davy, and A. Mignosi, *Optimization of Microphone Array Wall-Mountings in Closed-Section Wind Tunnels,* in *16th AIAA/CEAS Aeroacoustics Conference, Stockholm, Sweden* (2010) AIAA paper 2010–3738.

[38] T. Sinnige, B. Della Corte, R. de Vries, F. Avallone, R. Merino-Martinez, D. Ragni, G. Eitelberg, and L. L. M. Veldhuis, *Alleviation of Propeller–Slipstream–Induced Unsteady Pylon Loading by a Flow–Permeable Leading Edge,* Journal of Aircraft **56**, 1214 (2019), DOI: 10.2514/1.C035250.

[39] C. P. VanDercreek, R. Merino-Martinez, P. Sijtsma, and M. Snellen, *Evaluation of the effect of microphone cavity geometries on acoustic imaging in wind tunnels,* Applied Acoustics **181**, 1 (2021).

[40] H. Bento, C. VanderCreek, F. Avallone, D. Ragni, P. Sijtsma, and M. Snellen, *Wall treatments for aeroacoustic measurements in closed wind tunnel test sections,* in *29th AIAA/CEAS Aeroacoustics Conference, June 12 – 16 2023, San Diego, CA, USA* (2023) AIAA paper 2023–4162.

[41] Y. Hinssen, R. Merino-Martinez, and N. Moonen, *Enhancement of aeroacoustic testing in closed-section wind tunnels,* in *10th Berlin Beamforming Conference, June 10 – 11 2024, Berlin, Germany* (GFaI, e.V., Berlin, 2024) BeBeC–2024–S06.

[42] G.R.A.S. Sound & Vibration – 40PH CCP Free–field array microphone, *http://www.gras.dk/products/special-microphone/array-microphones/product/178-40ph,* Accessed in March 2017.

[43] S. Luesutthiviboon, A. Malgoezar, M. Snellen, P. Sijtsma, and D. G. Simons, *Improving Source Discrimination Performance by Using an Optimized Acoustic Array and Adaptive High–Resolution CLEAN–SC Beamforming,* in *7th Berlin Beamforming Conference, March 5 – 6 2018, Berlin, Germany* (GFaI, e.V., Berlin, 2018) BeBeC–2018–D07.

[44] G.R.A.S. Sound & Vibration – 42AA Pistonphone class 1, *https://www.gras.dk/products/calibration-equipment/reference-calibrator/product/255-42aa,* Accessed in March 2017.

[45] Visaton – Speaker K 50 SQ – 8 Ohm, *http://www.visaton.de/en/products/fullrange-systems/k-50-sq-8-ohm,* Accessed in March 2017.

[46] B. D. van Veen and K. M. Buckley, *Beamforming: A Versatile Approach to Spatial Filtering,* IEEE ASSP Magazine **5**, 4 (1988).

[47] R. Merino-Martinez, P. Sijtsma, and M. Snellen, *Inverse Integration Method for Distributed Sound Sources,* in *7th Berlin Beamforming Conference, March 5 – 6 2018, Berlin, Germany* (GFaI, e.V., Berlin, 2018) BeBeC–2018–S07.

[48] E. Sarradj, G. Herold, P. Sijtsma, R. Merino-Martinez, A. M. N. Malgoezar, M. Snellen, T. F. Geyer, C. J. Bahr, R. Porteous, D. J. Moreau, and C. J. Doolan, *A microphone array method benchmarking exercise using synthesized input data,* in *23rd AIAA/CEAS Aeroacoustics Conference, June 5 – 9 2017, Denver, CO, USA* (2017) AIAA paper 2017–3719.

[49] C. J. Bahr, W. M. Humphreys, D. Ernst, T. Ahlefeldt, C. Spehr, A. Pereira, Q. Leclère, C. Picard, R. Porteus, D. J. Moreau, J. Fischer, and C. J. Doolan, *A comparison of microphone phased array methods applied to the study of airframe noise in wind tunnel testing,* in *23rd AIAA/CEAS Aeroacoustics Conference, June 5 – 9 2017, Denver, CO, USA* (2017) AIAA paper 2017–3718.

[50] Q. Leclère, A. Pereira, C. Bailly, J. Antoni, and C. Picard, *A unified formalism for acoustic imaging based on microphone array measurements,* International Journal of Aeroacoustics **16**, 431 (2017), SAGE Publications Ltd. London, United Kingdom.

[51] R. Merino-Martinez, S. Luesutthiviboon, R. Zamponi, A. Rubio Carpio, D. Ragni, P. Sijtsma, M. Snellen, and C. Schram, *Assessment of the accuracy of microphone array methods for aeroacoustic measurements,* Journal of Sound and Vibration **470**, 1 (2020).

[52] E. Sarradj, *A generic approach to synthesize optimal array microphone arrangements,* in *6th Berlin Beamforming Conference, February 29 – March 1 2016, Berlin, Germany* (GFaI, e.V., Berlin, 2016) BeBeC–2016–S4.

[53] P. Sijtsma, *CLEAN based on spatial source coherence,* International Journal of Aeroacoustics **6**, 357 (2007), SAGE Publications Ltd. London, United Kingdom.

[54] P. Sijtsma, R. Merino-Martinez, A. M. N. Malgoezar, and M. Snellen, *High–Resolution CLEAN–SC: Theory and Experimental Validation,* International Journal of Aeroacoustics **16**, 274 (2017), SAGE Publications Ltd. London, United Kingdom.